Well Test Analysis of a Horizontal Well in a Bounded Anisotropic Oil and Gas Reservoir with a Sealed Bottom and a Constant-Pressure Boundary

Bakary L. Marong[1], Cherif Ahmat Tidiane Aidara[1], and Ebrima Njie[2]

[1] Mathematics Unit, Division of Physical and Natural Sciences, School of Arts and Sciences, University of The Gambia

[2]Department of Mathematics, Kent State University, Ohio, United States

Abstract

In this study, a horizontal well in anisotropic petroleum oil and gas reservoir with a sealed bottom and constant-pressure boundary is being investigated. The flow of petroleum oil and gas is governed by equation of continuity Darcy's law and equations of state. The combination of the above three equations gives a diffusivity equation. Early radial flow, early linear flow, pseudo radial flow and late linear flow were solved by integration. The number of parameters is reduced and the results were processed by the method of cubic spline interpolation using MATLAB. This research shows that at late linear flow period, the dimensionless time is inversely proportional to both dimensionless reservoir width and dimensionless height, but there is a constant pressure which indicates that the production of petroleum oil and gas is very low at late linear flow. Therefore the producing well is shut down for a build up. The research's conclusions are relevant to maximizing well productivity as well as to petroleum engineering.

1. **Introduction**

The ever-growing transportation, industrial, residential, commercial, and electrical sectors have raised significant concerns for the world economies over the need for fuel. Production continues to be under strain as large amounts of oil and its refined products are consumed daily. The demand for this valuable resource must remain strong in order to support a functioning global economy. The process of guaranteeing that more oil is produced involves several different steps, including seismic surveys, exploration, drilling, development, assessment, appraisals, production, and recovery. Pressure transient analysis is a critical step in this process. When an oil and gas reservoir has been found and its reserves have been determined to be viable, it is crucial to make sure that the output is maximized. The location, capacity, and amount of the drainage volume will all be taken into consideration when deciding what kind of oil well to drill.

Pressure transient analysis is mainly used for reservoir characterization in exploration and appraisal stage. During an exploration well test, hydrocarbon is produced for the first time and flared via a temporary facilities to evaluate the potential and reserves of oil and gas field. This is too expensive, and it involves high safety and environmental risks. A poorly performed well test could lead to a disastrous field development and huge financial loses.
While more value could be extracted by applying modern Well test analysis tools and techniques, Well test analysis can also be used to monitor the well and reservoir performance and understand the causes of performance deviation. For fractured wells, it will help to evaluate the actual fracture dimension and obtain permeability and initial pressure. For water injectors, pressure transient analysis will help to ensure no excessive frac growth, cap

rock integrity and water containment in the reservoir.

A petroleum reservoir is a subsurface accumulation of hydrocarbons contained in porous or fractured rock formations. A reservoir is formed when ancient plant materials is created in surrounding rock by the presence of high heat and pressure in the earth's crust. Types of petroleum oil reservoirs are standard oil reservoirs which is mostly crude oil with some water and gas. Volatile oil reservoirs contain high amounts of corrosive gas in addition to oil and water. Dry Gas Reservoirs which is mostly natural gas with some water vapor. Gas Condensate Reservoirs contains heavy hydrocarbons that turn into NGL's once brought to the surface.
A constant pressure boundary is a boundary that provides pressure support. This kind of boundary usually occurs in reservoirs with aquifer support. Steady state flow signifies that a constant pressure boundary has been reached.

3. **Mathematical Formulation**

With constant pressure boundaries and sealed bottom of reservoir length x_e in the x-direction, reservoir width y_e in the y-direction, and reservoir thickness h in the z-direction. Since it is assumed that the reservoir is homogeneous and anisotropic, the permeability of the formation differs from the permeability of the axial direction. The Petroleum oil well is situated in the reservoir's middle.

Our previous articles differs from the current one, because the current one consider anisotropic homogeneous reservoir, where the permeability along the x, y, and z boundaries differs, while the previous two published articles

studied Isotropic reservoir where the permeability along the three boundaries are the same.

Many studies overlooked the anisotropic homogenous reservoir with a sealed bottom and constant pressure boundaries. This study has thus investigated the well test analysis of a horizontal petroleum oil and gas well with a constant pressure boundaries and a sealed bottom of anisotropic reservoir where the four flow regimes were solved by integration. It is also evident that analyzing a horizontal well is more difficult than analyzing a vertical one.

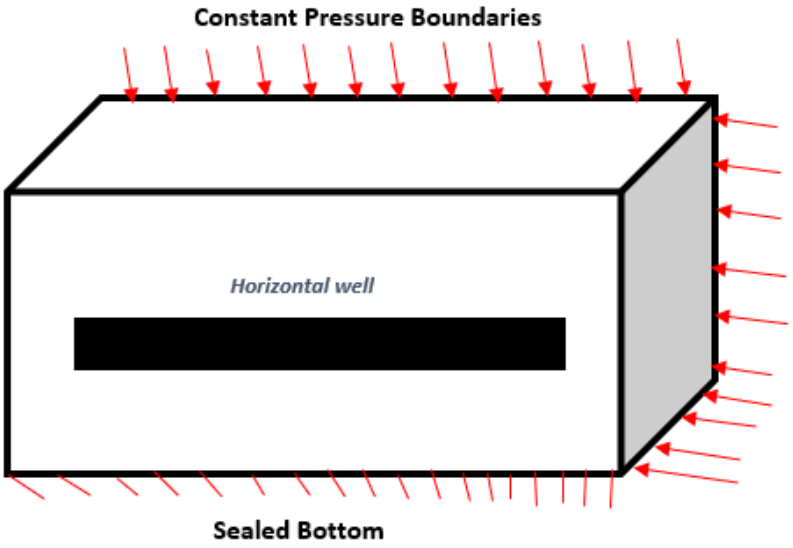

Figure 1: Physical Model of a Horizontal oil and gas well with sealed bottom and Constant Pressure at y and z-boundaries

The governing equations are the equation of continuity, equations of state, and Darcy's law. Equation$(1), (2), and (5)$ combined gives the Diffusivity equation which is equation (8)

$$\frac{\partial(\rho u_x)}{\partial x}+\frac{\partial(\rho u_y)}{\partial y}+\frac{\partial(\rho u_z)}{\partial z} = -\frac{\partial(\rho\phi)}{\partial t} \tag{1}$$

From the above equation ρ is the density of the fluid, ϕ is the porosity of the formation and both are position of x,y,z and t. Further u_x,u_y and u_z are components of velocity in the x, y, and z directions, respectively.

The Darcy's law is the central concept in the study of fluid flow in porous media. Darcy's law describes how liquid moves through a porous medium under the influence of a pressure gradient. The flow rate and pressure are related by a constant flow rate q a core of length L and cross-sectional area

A, as shown in the figure (2)

$$q = \frac{KA}{\mu}\frac{\Delta P}{L} \tag{2}$$

The flow rate q is in m^3/s, the cross sectional area A is in meter square, the length L is in meters, the pressures P_1 and P_2 are in pascals, the permeability k is in meters , and the viscosity μ is in poise. This study had contributed to Darcy's law by adding porosity and capillary pressure on the right hand side.

$$q = \frac{KA}{\mu}\frac{\Delta P}{L} + \frac{V_{void}}{V_{bulk}} \tag{3}$$

Equation (3) is the development of Darcy's law, by adding of porosity. Here V_{void} is the pore volume in m^3 and V_{bulk} is the bulk volume.

$$q = \frac{KA}{\mu}\frac{\Delta P}{L} + \frac{2\sigma cos\theta}{r} \tag{4}$$

Equation (4) is the development of Darcy's law by adding of capillary pressure, and r is the pore radius, σ is the surface tension in Milli-Newtons per meter and θ is the contact angle in degrees.

The equation of state relates the density of the fluid to the pressure and thus considering a slightly compressible fluid, the fluid compressibility, c is given by;

$$c = \frac{1}{\rho} \times \frac{\partial \rho}{\partial p} \tag{5}$$

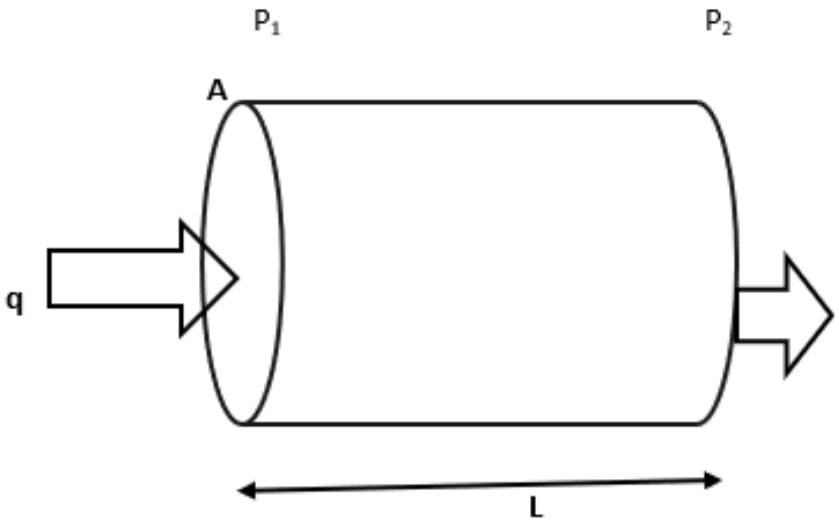

Figure 2: Linear flow through a core sample

This study had contributed to the equation of state by adding entropy and enthalpy on the right hand side.

$$c = \frac{1}{\rho} \times \frac{\partial \rho}{\partial P} + \frac{Q}{P} \tag{6}$$

Equation (6) is the development of equation of state by adding of entropy, where Q is the heat transfer and T is the reservoir temperature.

$$c = \frac{1}{\rho} \times \frac{\partial \rho}{\partial P} + E + PV \tag{7}$$

Equation (7) is the development of equation of state by adding enthalpy, where E is the internal energy, P is the pressure and V the volume.

Unsteady flow of fluids is governed by diffusivity equation, which is a three-

dimensional partial differential equation that describes the flow of petroleum oil and gas through porous media given as

$$k_x\frac{\partial^2 P}{\partial x^2}+k_y\frac{\partial^2 P}{\partial y^2}+k_z\frac{\partial^2 P}{\partial z^2}=\phi\mu c_t\frac{\partial P}{\partial t} \tag{8}$$

where k_x is the permeability along the x-direction, k_y is the permeability along the y-boundary, k_z is the permeability along the z-boundary, P is the pressure, c_t is the total compressible μ is the reservoir viscosity and ϕ is the reservoir porosity.

This study used Source and Green's function to model dimensionless pressure P_D and dimensionless pressure derivative $P_{D'}$

Well Test Analysis Models

This study used Green's and Source functions to modeled dimensionless pressure and dimensionless pressure derivative of a reservoir with sealed bottom and constant pressure along the y and z-boundaries. This study suggested four flow periods that is early radial flow, early linear flow, pseudoradial flow and late linear flow.

Early Radial Flow

This flow period occurs when none of the boundaries is been sensed by the flow. It is the situation when the well is first made available for production.

$$P_D=2\pi h_D\int_0^{t_D}\frac{1}{2}[erf(\frac{\sqrt{\frac{k}{k_x}}+(x_D-x_{wD})}{2\sqrt{\tau_D}})+erf(\frac{\sqrt{\frac{k}{k_x}}+(x_D-x_{wD})}{2\sqrt{\tau_D}})$$
$$\times\frac{1}{2\sqrt{\pi t_D}}[\sqrt{\frac{k}{k_y}}e^{-\frac{(y_D-y_{wD})^2}{4\tau_D}}]\times\frac{1}{2\sqrt{\pi t_D}}[\sqrt{\frac{k}{k_z}}e^{-\frac{(z_D-z_{wD})^2}{4\tau_D}}]\}d\tau_D \tag{9}$$

$$P_{D'}=2\pi h_D\{\frac{1}{2}[erf(\frac{\sqrt{\frac{k}{k_x}}+(x_D-x_{wD})}{2\sqrt{t_D}})+erf(\frac{\sqrt{\frac{k}{k_x}}+(x_D-x_{wD})}{2\sqrt{t_D}})$$
$$\times\frac{1}{2\sqrt{\pi t_D}}[\sqrt{\frac{k}{k_y}}e^{-\frac{(y_D-y_{wD})^2}{4t_D}}]\times\frac{1}{2\sqrt{\pi t_D}}[\sqrt{\frac{k}{k_z}}e^{-\frac{(z_D-z_{wD})^2}{4t_D}}]\} \tag{10}$$

Early Linear Flow

Early linear flow period occurs, when x and y-boundaries are not been encountered by the flow, while z-boundary encounters a constant pressure.

$$P_D = 2\pi h_D \int_0^{t_D} \tfrac{1}{2}[erf(\tfrac{\sqrt{\frac{k}{k_x}}+(x_D-x_{wD})}{2\sqrt{\tau_D}}) + erf(\tfrac{\sqrt{\frac{k}{k_x}}+(x_D-x_{wD})}{2\sqrt{\tau_D}})$$
$$\times \tfrac{1}{2\sqrt{\pi t_D}}[\sqrt{\frac{k}{k_y}} e^{-\frac{(y_D-y_{wD})^2}{4\tau_D}}]$$
$$\times[\tfrac{1}{h_D}\sum_{l=1}^{\infty} \exp(-\tfrac{(2n-1)^2\pi^2\tau_D}{4h_D^2}) \sin\tfrac{(2n-1)\pi z_{wD}}{2h_D} \sin\tfrac{(2n-1)}{2_{hD}}]\}d\tau_D \quad (11)$$

Pseudoradial Flow

The flow along the y and z-boundaries encounters a constant pressure, while x-boundary does not.

$$P_D = 2\pi h_D \int_0^{t_D} \tfrac{1}{2}[erf(\tfrac{\sqrt{\frac{k}{k_x}}+(x_D-x_{wD})}{2\sqrt{\tau_D}}) + erf(\tfrac{\sqrt{\frac{k}{k_x}}+(x_D-x_{wD})}{2\sqrt{\tau_D}})$$
$$\times \tfrac{1}{y_{eD}}[1 + 2\sum_{m=1}^{\infty} \exp(-\tfrac{m^2\pi^2\tau_D}{{y_{eD}}^2}) \cos\tfrac{m\pi y_{wD}}{y_{eD}} \cos\tfrac{m\pi y_D}{y_{eD}}]$$
$$\times[\tfrac{1}{h_D}\sum_{l=1}^{\infty} \exp(-\tfrac{(2n-1)^2\pi^2\tau_D}{4{h_D}^2}) \sin\tfrac{(2n-1)\pi z_{wD}}{2h_D} \sin\tfrac{(2n-1)}{2h_D}]d\tau_D \quad (12)$$

Late Linear Flow

Late linear flow happens when there is a constant pressure at all the boundaries

$$P_D = 2\pi h_D \int_0^{t_D} [\tfrac{8}{\pi}\sum_{n=1}^{\infty} \tfrac{1}{2n+1} \exp(-\tfrac{(2n+1)^2\pi^2\tau_D}{4{x_{eD}}^2}) \sin\tfrac{(2n+1)\pi x_{wD}}{2x_{eD}}$$
$$\cos\tfrac{(2n+1)\pi x_D}{2x_{eD}} \cos\tfrac{(2n+1)\pi x_D}{2x_{eD}}]\times\tfrac{1}{y_{eD}}[1+2\sum_{m=1}^{\infty} \exp(-\tfrac{m^2\pi^2\tau_D}{{y_{eD}}^2}) \cos\tfrac{m\pi y_{wD}}{y_{eD}} \cos\tfrac{m\pi y_D}{y_{eD}}]$$
$$\times\tfrac{1}{h_D}[\sum_{l=1}^{\infty} \exp(-\tfrac{(2n-1)^2\pi^2\tau_D}{4{h_D}^2}) \sin\tfrac{(2n-1)\pi z_{WD}}{2h_D} \sin\tfrac{(2n-1)}{2h_D}]d\tau_D \quad (13)$$

Integration of the flow regimes

The integration of early radial, early linear, pseudo radial and late linear flow are illustrated below.

Early radial flow

This study integrated early radial flow to reduced the number of parameters by considering all the boundaries to be infinite acting.

$$P_D = 2\pi h_D \int_0^{t_D} \{\frac{1}{2} erf(\frac{\sqrt{\frac{k}{k_x}}+(x_D-x_{wD})}{2\sqrt{t_D}}) + erf(\frac{\sqrt{\frac{k}{k_x}}+(x_D-x_{wD})}{2\sqrt{t_D}}) \times \frac{1}{2\sqrt{\pi t_D}}[\sqrt{\frac{k}{k_y}} e^{-\frac{(y_D-y_{wD})^2}{4t_D}}] \times \frac{1}{2\sqrt{\pi t_D}}[\sqrt{\frac{k}{k_z}} e^{-\frac{(z_D-z_{wD})^2}{4t_D}}]\} d\tau_D \quad (14)$$

$$\beta = erf(\frac{\sqrt{\frac{k}{k_x}}+(x_D-x_{wD})}{2\sqrt{\tau_D}}) + erf(\frac{\sqrt{\frac{k}{k_x}}+(x_D-x_{wD})}{2\sqrt{\tau_D}}) \quad (15)$$

$$P_D = 2\pi h_D \int_0^{t_D} \{\frac{1}{2\sqrt{\pi t_D}}[\sqrt{\frac{k}{k_y}} e^{-\frac{(y_D-y_{wD})^2}{4t_D}}] \times \frac{1}{2\sqrt{\pi t_D}}[\sqrt{\frac{k}{k_z}} e^{-\frac{(z_D-z_{wD})^2}{4t_D}}]\} d\tau_D \quad (16)$$

$$u = \frac{r_{wD}^2}{4t_D}$$

$$P_D = -\frac{h_D}{4} Ei(-\frac{r_{wD^2}}{4t_D}) \quad (17)$$

where $h_D = \frac{1}{L_D}$

$$P_D = -\frac{1}{4L_D} Ei(-\frac{r_{wD^2}}{4_{tD}}) \quad (18)$$

$$P_D' = \frac{1}{4L_D} exp(-\frac{r_{wD^2}}{4t_D}) \quad (19)$$

Early Linear Flow

This study integrated the early linear flow period to reduce the parameters.

$$P_D = 2\pi h_D \int_0^{t_D} \{\tfrac{1}{2}[erf(\tfrac{\sqrt{\frac{k}{k_x}}+(x_D-x_{wD})}{2\sqrt{\tau_D}}) + erf(\tfrac{\sqrt{\frac{k}{k_x}}+(x_D-x_{wD})}{2\sqrt{\tau_D}})]$$
$$\times \tfrac{1}{2\sqrt{\pi t_D}}\sqrt{\tfrac{k}{k_y}}\exp[-\tfrac{(y_D-y_{wD})^2}{4\tau_D}]$$
$$\times \tfrac{1}{h_D}[1+2\textstyle\sum_{l=1}^{\infty}\exp(-\tfrac{(2n-1)^2\pi^2\tau_D}{4{h_D}^2})\sin\tfrac{(2n-1)\pi z_{wD}}{2h_D}\sin\tfrac{(2n-1)\pi z_D}{2h_D}]\}d\tau_D \quad (20)$$

where k is the permeability at the formation, k_x is the permeability along the x-boundary, n is the number of wells and this study considers only one well,

y_D dimensionless width, y_{wD} dimensionless well bore width.

$$\beta = erf(\tfrac{\sqrt{\frac{k}{k_x}}+(x_D-x_{wD})}{2\sqrt{\tau_D}})+erf(\tfrac{\sqrt{\frac{k}{k_x}}+(x_D-x_{wD})}{2\sqrt{\tau_D}}) \quad (21)$$

$$P_D = \tfrac{\pi}{\sqrt{\pi t_D}}\int_0^{t_D}[1+2\textstyle\sum_{l=1}^{1}\exp(-\tfrac{\pi^2\tau_D}{4{h_D}^2})\sin\tfrac{\pi z_{wD}}{2h_D}\sin\tfrac{\pi z_D}{2h_D}]d\tau_D \quad (22)$$

$$P_D = \sqrt{\pi}\int_0^{t_D} 1+2\exp(-\tfrac{\pi^2\tau_D}{4{h_D}^2})\tfrac{d\tau_D}{\sqrt{\tau_D}} \quad (23)$$

By substituting the upper and the lower limit, we obtained equation (24)

$$P_D = \sqrt{\pi}[\sqrt{t_D}-2\tfrac{4{h_D}^2}{\pi^2}e^{-\frac{\pi^2}{4{h_D}^2}}\sqrt{t_D}] \quad (24)$$

$$P_{D'} = t_D\tfrac{\partial P_D}{\partial t_D}$$

(25)

$$P_{D'} = \sqrt{\pi}[1+2\exp(-\tfrac{\pi^2\tau_D}{4{h_D}^2})]\sqrt{t_D} \quad (26)$$

$$P_{D'} = \sqrt{\pi t_D}[1+2e^{-\frac{\pi^2\tau_D}{4{h_D}^2}}\sqrt{t_D}] \quad (27)$$

Pseudoradial flow

This study has integrated the pseudoradial flow period to reduce the parameters.

$$P_D = 2\pi h_D \int_0^{t_D} \{\tfrac{1}{2}[erf(\tfrac{\sqrt{\frac{k}{k_x}}+(x_D-x_{wD})}{2\sqrt{\tau_D}}) + erf(\tfrac{\sqrt{\frac{k}{k_x}}+(x_D-x_{wD})}{2\sqrt{\tau_D}})]$$
$$\times \tfrac{1}{y_{eD}}[1 + 2\sum_{m=1}^{\infty} \exp(-\tfrac{m^2\pi^2}{\tau}_D y_{eD^2}) \cos\tfrac{m\pi y_{wD}}{y_{eD}} \cos\tfrac{m\pi y_D}{y_{eD}}]$$
$$\times\tfrac{1}{h_D}[1+2\sum_{l=1}^{\infty} \exp(-\tfrac{(2n-1)^2\pi^2\tau_D}{4h_{D^2}}) \sin\tfrac{(2n-1)\pi z_{wD}}{2h_D} \sin\tfrac{(2n-1)\pi z_D}{2h_D}]\}d\tau_D \tag{28}$$

$$\beta = erf(\tfrac{\sqrt{\frac{k}{k_x}}+(x_D-x_{wD})}{2\sqrt{\tau_D}})+erf(\tfrac{\sqrt{\frac{k}{k_x}}+(x_D-x_{wD})}{2\sqrt{\tau_D}}) \tag{29}$$

$$P_D = \tfrac{2\pi}{y_{eD}} \int_0^{t_D} [(1 + 2\exp(-\tfrac{\pi^2\tau_D}{y_{eD^2}}) \cos\tfrac{\pi y_{wD}}{y_{eD}} \cos\tfrac{\pi y_D}{y_{eD}})$$
$$\times(1+2\exp(-\tfrac{\pi^2\tau_D}{4h_{D^2}}) \sin\tfrac{\pi z_{wD}}{2h_D} \sin\tfrac{\pi z_D}{2h_D})]d\tau_D \tag{30}$$

$$P_D = \tfrac{2\pi}{y_{eD}} \int_0^{t_D} [(1 + 2\exp(-\tfrac{\pi^2\tau_D}{y_{eD^2}}) \cos\tfrac{\pi}{2} \cos\tfrac{\pi}{2})$$
$$\times(1+2\exp(-\tfrac{\pi^2\tau_D}{4h_{D^2}}) \sin\tfrac{\pi z_{wD}}{2h_D} \sin\tfrac{\pi z_D}{2h_D})]d\tau_D \tag{31}$$

$$P_D = \tfrac{2\pi}{y_{eD}} \int_0^{t_D} [(1+2\exp(-\tfrac{\pi^2\tau_D}{y_{eD^2}})0)\times(1+2\exp(-\tfrac{\pi^2\tau_D}{4h_{D^2}}) \sin\tfrac{\pi}{2} \sin\tfrac{\pi}{2})]d\tau_D \tag{32}$$

$$P_D = \tfrac{2\pi}{y_{eD}} \int_0^{t_D} [(1+2\exp(-\tfrac{\pi^2\tau_D}{4h_{D^2}}))]d\tau_D \tag{33}$$

$$P_D = \tfrac{2\pi}{y_{eD}} \int_0^{t_D} (1+2e^{-}\tfrac{\pi^2}{4h_{D^2}}\tau_D)d\tau_D \tag{34}$$

By substituting the upper and the lower limit, we obtained equation (35)

$$P_D = \tfrac{2\pi}{y_{eD}}[t_D-2\tfrac{4h_{D^2}}{\pi^2}e^{-}\tfrac{\pi^2}{4h_{D^2}}t_D] \tag{35}$$

$$P_{D'} = t_D\tfrac{\partial P_D}{\partial t_D} \tag{36}$$

$$P_{D'} = \tfrac{2\pi t_D}{y_{eD}}(1+2e^{-}\tfrac{\pi^2}{4h_{D^2}}\tau_D) \tag{37}$$

Integration of Late Linear Flow

This study has integrated the Late Linear flow period to reduce the parameters.

$$P_D = 2\pi h_D \int_0^{t_D} \{[\tfrac{8}{\pi} \sum_{n=1}^{\infty} \tfrac{1}{2n+1} \exp(-\tfrac{(2n+1)^2\pi^2\tau_D}{4x_{eD^2}}) \sin \tfrac{(2n+1)\pi x_{wD}}{2x_{eD}} \cos \tfrac{(2n+1)\pi x_D}{2x_{eD}}$$
$$\cos \tfrac{(2n+1)\pi x_D}{2x_{eD}}] \times \tfrac{1}{y_{eD}}[1 + 2\sum_{m=1}^{\infty} \exp(-\tfrac{m^2\pi^2\tau_D}{y_{eD^2}}) \cos \tfrac{m\pi y_{wD}}{y_{eD}} \cos \tfrac{m\pi y_D}{y_{eD}}]$$
$$\times \tfrac{1}{h_D}[1+2\sum_{l=1}^{\infty} \exp(-\tfrac{(2n-1)\pi^2\tau_D}{4h_{D^2}}) \sin \tfrac{(2n-1)\pi z_{wD}}{2h_D} \sin \tfrac{(2n-1)\pi z_D}{2h_D}]\}d\tau_D \quad (38)$$

From equation (38) n is the number of wells, x_{eD} is the dimensionless reservoir length, y_{eD} dimensionless reservoir width, h_D dimensionless height.

$$P_D = \tfrac{2\pi}{y_{eD}} \int_0^{t_D} \{\tfrac{8}{\pi} \sum_{n=1}^{\infty} \tfrac{1}{2n+1} \exp(-\tfrac{(2n-1)^2\pi^2\tau_D}{4_{eD^2}}) \sin \tfrac{(2n+1)\pi x_{wD}}{2x_{eD}} \cos \tfrac{(2n+1)\pi x_D}{2x_{eD}}$$
$$\cos \tfrac{(2n+1)\pi x_D}{2x_{eD}} \times \tfrac{1}{y_{eD}}[1 + 2\sum_{m=1}^{\infty} \exp(-\tfrac{m^2\pi^2\tau_D}{y_{eD^2}}) \cos \tfrac{m\pi y_{wD}}{y_{eD}} \cos \tfrac{m\pi y_D}{y_{eD}}]$$
$$\times[1+2\sum_{l=1}^{\infty} \exp(-\tfrac{(2n-1)\pi^2\tau_D}{4h_{D^2}}) \sin \tfrac{(2n-1)\pi z_{wD}}{2h_D} \sin \tfrac{(2n-1)\pi z_D}{2h_D}]\}d\tau_D \quad (39)$$

$$P_D = \tfrac{2\pi}{y_{eD}} \int_0^{t_D} \{[\tfrac{8}{\pi} \sum_{n=1}^{1} \tfrac{1}{3} \exp(-\tfrac{\pi^2\tau_D}{4x_{eD^2}}) \sin \tfrac{3\pi x_{wD}}{2x_{eD}} \cos \tfrac{3\pi x_D}{2x_{eD}} \cos \tfrac{3\pi x_D}{2x_{eD}}]$$
$$\times \tfrac{1}{y_{eD}}[1 + 2\sum_{m=1}^{1} \exp(-\tfrac{\pi^2\tau_D}{y_{eD^2}}) \cos \tfrac{\pi y_{wD}}{y_{eD}} \cos \tfrac{\pi y_D}{y_{eD}}]$$
$$\times[1+2\sum_{l=1}^{1} \exp(-\tfrac{\pi^2\tau_D}{4h_{D^2}}) \sin \tfrac{\pi z_{wD}}{2h_D} \sin \tfrac{\pi z_D}{2h_D}]\}d\tau_D \quad (40)$$

$$r_{wD} = z_D - z_{wD}$$
$$P_D = \int_0^{t_D} ([\tfrac{1}{3} \exp(-\tfrac{\pi^2\tau_D}{4x_{eD^2}}) \sin \tfrac{3\pi}{2} \cos \tfrac{3\pi}{2} \cos \tfrac{3\pi}{2}]$$
$$\times[1+2\exp(-\tfrac{\pi^2\tau_D}{y_{eD^2}}) \cos \tfrac{\pi}{2} \cos \tfrac{\pi}{2}] \times [1+2\exp(-\tfrac{\pi^2\tau_D}{4h_{D^2}}) \sin \tfrac{\pi z_{wD}}{2h_D} \sin \tfrac{\pi z_D}{2h_D}])d\tau_D \quad (41)$$

$$P_D = \tfrac{16}{y_{eD}} \int_0^{t_D} [2\exp(-\tfrac{\pi^2\tau_D}{4h_{D^2}}) \times 1]d\tau_D \quad (42)$$

$$P_D = \tfrac{16}{y_{eD}} \int_0^{t_D} [2e^{-\tfrac{\pi^2}{4h_{D^2}}\tau_D}]d\tau_D \quad (43)$$

By substituting the upper and lower limits, we obtained equation (44)

$$P_D = \tfrac{16}{y_{eD}}[2e^{-\tfrac{\pi^2}{4h_{D^2}}t_D}] \quad (44)$$

$$P_D = \tfrac{16}{y_{eD}}[2\tfrac{4h_{D^2}}{\pi^2}e^{-\tfrac{\pi^2}{4h_{D^2}}t_D}] \quad (45)$$

$$P_{D'} = t_D \frac{\partial P_D}{\partial t_D} \tag{46}$$

$$P_{D'} = \frac{16 t_D}{y_{eD}} (2e^{-\frac{\pi^2}{4h_{D^2}}} \tau_D) \tag{47}$$

4. Results and Discussions

The results obtained are presented using graphs and a data table which is followed by a discussion.

$K = 20m^2$, $k_x = 18m^2$, $k_y = 14m^2$, $k_z = 16m^2$, $h = 36m$

$x_e = 500m$, $y_e = 300m$, $z_e = 100m$, $z_w = 50m$, $z = 75m$

From table 1, the length of the well has been stretched from $250m$ to $2250m$.

Table 1: Dimensionless parameters for varying L_D

$L(ft)$	250	500	750	1000	1250	1500	1750	2000	2250
L_D	3.660	7.3201	10.9801	14.6402	18.3002	21.9603	25.6203	29.2803	32.9404
h_D	0.3220	0.1610	0.1073	0.0805	0.0644	0.0537	0.0460	0.0402	0.0337
x_D	0.5	0.5	0.5	0.5	0.5	0.5	0.5	0.5	0.5
z_{wD}	0.4472	0.2236	0.1491	0.1118	0.0894	0.0746	0.0638	0.0559	0.0496
x_{wD}	0.5	0.5	0.5	0.5	0.5	0.5	0.5	0.5	0.5
y_{wD}	1.4343	0.7172	0.4781	0.3586	0.2869	0.2391	0.2049	0.1793	0.1594
z_D	0.6708	0.3354	0.2236	0.1677	0.1342	0.1118	0.0958	0.0839	0.0745
x_{eD}	4.2164	2.1082	1.4055	1.0541	0.8433	0.7027	0.6023	0.5271	0.4685
y_D	1.4343	0.7172	0.4781	0.3586	0.2869	0.2391	0.2049	0.1793	0.1594
z_{eD}	0.8944	0.4472	0.2981	0.2236	0.1789	0.1491	0.1278	0.1118	0.0994
y_{eD}	2.8685	1.4343	0.9562	0.7171	0.5737	0.4781	0.4098	0.3586	0.3187
r_{wD}	0.2236	0.1118	0.0745	0.0559	0.0448	0.0372	0.032	0.028	0.0249

This result shows as dimensionless length increases both the pay thickness and the reservoir length decreases. This shows that dimensionless length of the oil well is inversely proportional to both the well pay thickness and the dimensionless reservoir width.

In figure (3), as the length of the well is stretched both the dimensionless length, dimensionless source coordinate in the z-direction, dimensionless source coordinate in the y-direction, dimensionless heigth, dimensionless reservoir length and dimensionless reservoir width decreases. This results

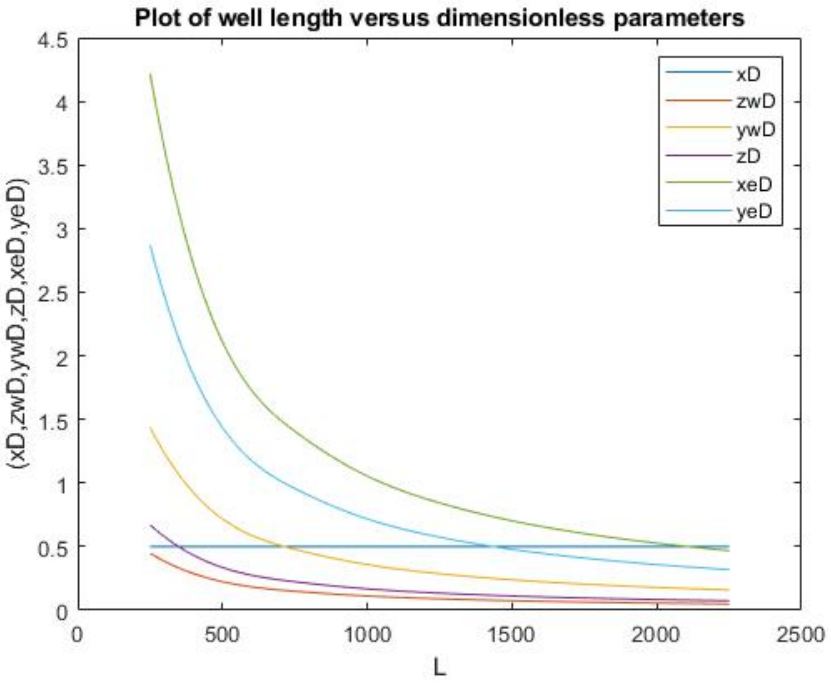

Figure 3: Variation of well length with dimensionless length, dimensionless source coordinate in the z-direction, dimensionless source coordinatein the y-direction, dimensionless height, dimensionless reservoir length and dimensionless reservoir width

shows that well length is inversely proportional to most of the dimensionless parameters.

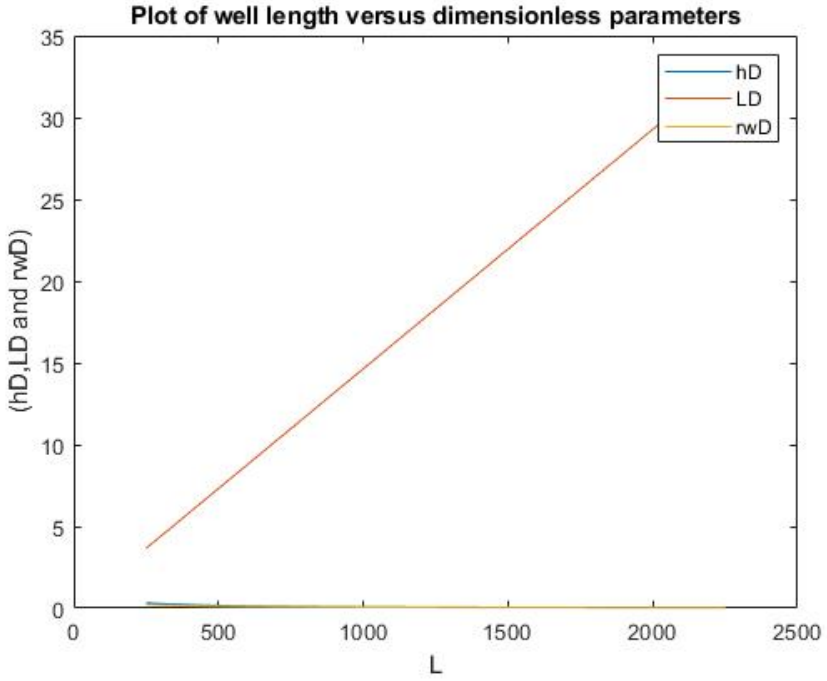

Figure 4: Variation of well length with dimensionless well length, pay thickness and dimensionless well bore radius

In figure 4, as the well length stretches, the dimensionless well length increases, where as both the dimensionless height and dimensionless well bore radius coincide towards the walls of the well. This results shows that well length is directly proportional to the dimensionless well length, but the dimensionless height and dimensionless well bore radius get attached to the walls of the well.

Table 2: The Increased of Dimensionless time and Dimensionless Pressure with a constant Dimensionless pressure derivative during early radial flow

t_D	P_D	$P_{D'}$
$1.0e-01$	0.0197	0.0070
$2.0e-01$	0.0300	0.00689
$3.0e-01$	0.0367	0.0068
$4.0e-01$	0.0417	0.0068
$5.0e-01$	0.0458	0.0068
$6.0e-01$	0.0491	0.0068
$7.0e-01$	0.0519	0.0068
$8.0e-01$	0.0545	0.0068
$9.0e-01$	0.0567	0.0068

In figure 5, as dimensionless time increases, dimensionless pressure increases, dimensionless pressure derivative is a constant. This results shows that dimensionless time is directly proportional to dimensionless pressure. During this flow period is the period when the well is initially open for production. The production of petroleum oil and gas is highest at this period. Early radial flow has a zero gradient.

Figure 6 is the graph of dimensionless pressure against dimensionless time. It has showed that as dimensionless pressure increased, dimensionless time also increased. This result shows that dimensionless pressure is directly proportional to dimensionless time when the well is initially opened for production.

Figure 7 is the graph of dimensionless pressure derivative against dimen-

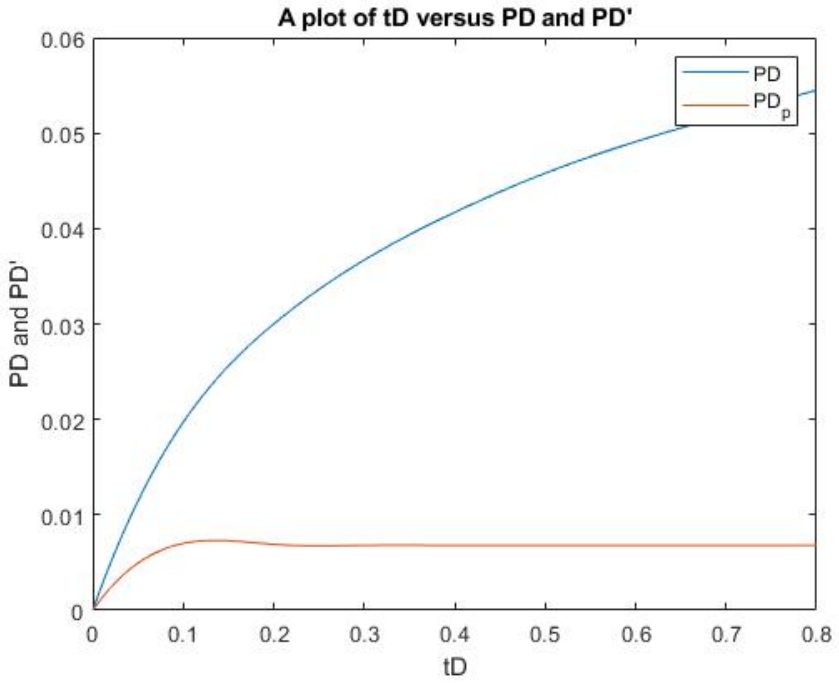

Figure 5: Variation of Dimensionless time with Dimensionless pressure and Dimensionless pressure derivative

sionless time, it has been demonstrated from the figure as dimensionless time increases, dimensionless pressure derivative becomes a constant. This implies that dimensionless pressure derivative has a slope of zero.

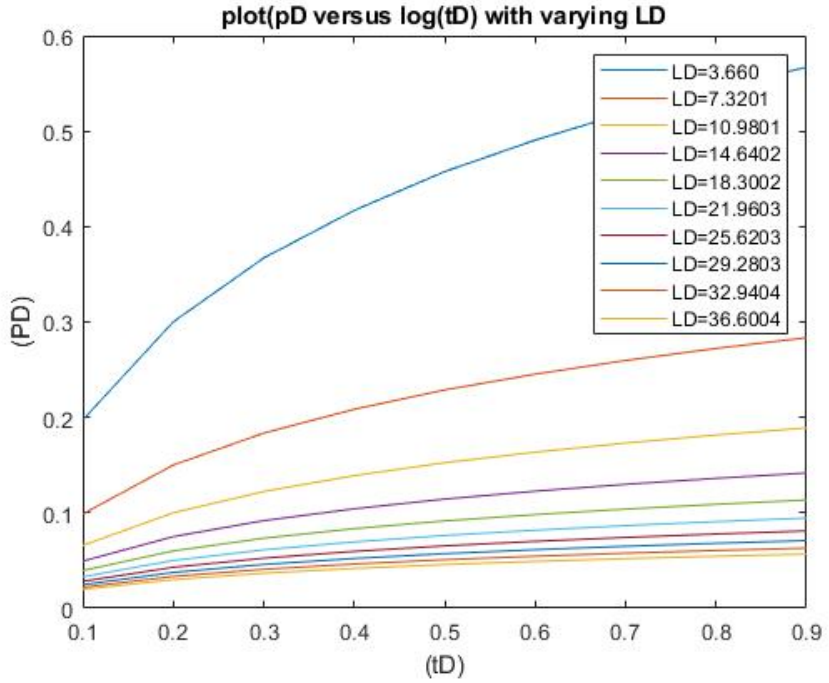

Figure 6: Dimensionless time and Dimensionless Pressure with a varying L_D

Table 3: The values of tD, PD and PD' during Early Linear flow

t_D	0	0.10	0.20	0.30	0.40	0.50	0.60	0.70	0.80
PD	0	0.560	0.792	0.972	1.121	1.253	1.374	1.484	1.585
PD'	0	0.561	0.793	0.971	1.121	1.253	1.373	1.483	1.585

In figure 8, as dimensionless time increases, dimensionless pressure increases and dimensionless pressure derivative is a straight line, which implies that early linear flow has a gradient of 1. This results shows that dimensionless time is directly proportional to dimensionless pressure. The production of petroleum, oil and gas is higher.

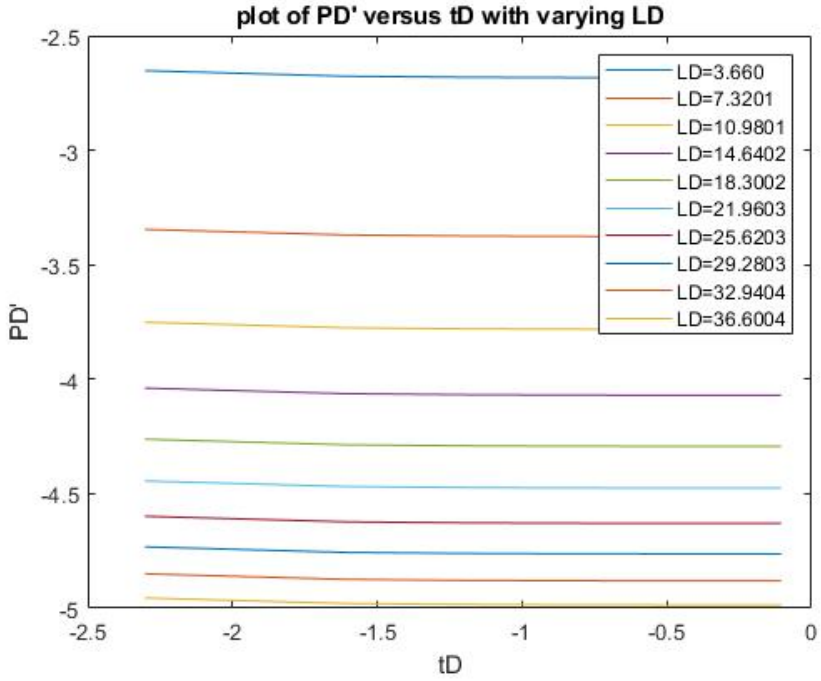

Figure 7: Dimensionless time and Dimensionless Pressure derivative with a varying L_D

In figure 9, as dimensionless time increases, dimensionless pressure increases, dimensionless pressure derivative is a constant and dimensionless height decreases. This results shows that dimensionless time is directly proportional to dimensionless pressure and inversely proportional to dimensionless height and it has a gradient of 1.

Table 4: The values of tD, PD and $PD^{'}$ during pseudoradial flow

t_D	0	0.10	0.20	0.30	0.40	0.50	0.60	0.70	0.80
PD	0	0.219	1.314	2.629	4.381	6.571	9.200	12.266	15.773
$PD^{'}$	0	0.044	0.263	0.789	1.752	3.286	5.521	8.587	12.619

In figure 10, as dimensionless time increases, dimensionless pressure increases and dimensionless pressure derivative is not a perfect straight line. This results shows that dimensionless time is directly proportional to dimensionless

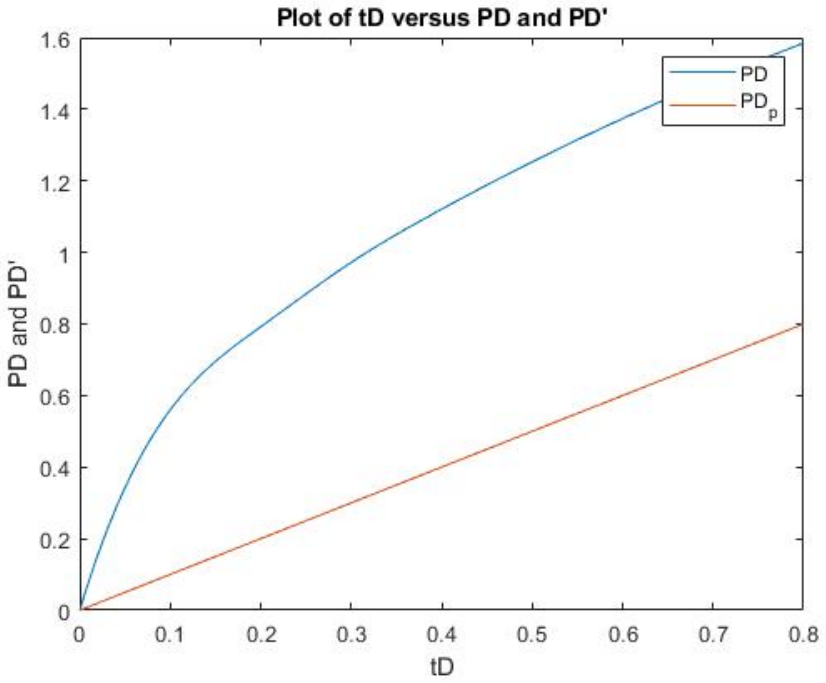

Figure 8: Variation of Dimensionless time with Dimensionless Pressure and Dimensionless Pressure derivative at early linear flow

pressure. During pseudo radial flow period, the production of petroleum, oil and gas is better. Pseudo radial flow has a gradient of $\frac{1}{2}$

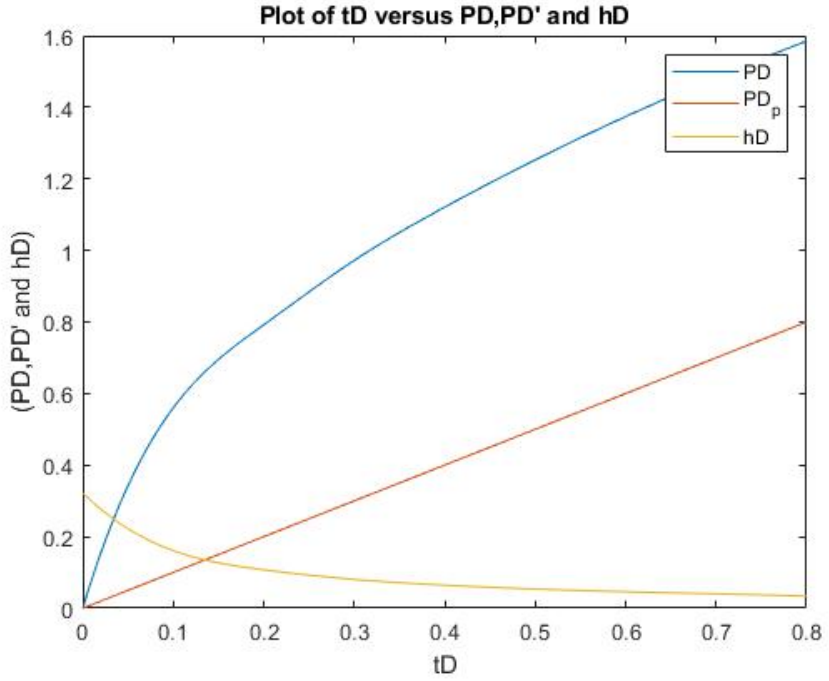

Figure 9: Variation of Dimensionless time with Dimensionless Pressure, Dimensionless Pressure derivative and pay thickness at early linear flow

In figure 11, as dimensionless time increases, dimensionless pressure increases, dimensionless pressure derivative is not a perfect straight line, dimensionless reservoir width decreases and dimensionless height is a constant. This results shows that dimensionless time is directly proportional to dimensionless pressure and inversely proportional to dimensionless reservoir width.

Table 5: The values of tD, PD and $PD^{'}$ during late linear flow

t_D	0	0.10	0.20	0.30	0.40	0.50	0.60	0.70	0.80
PD	0	1.0×10^{-43}	2.5×10^{-95}	1.4×10^{-167}	1.4×10^{-260}	7.8×10^{-374}	1.1×10^{-508}	2.7×10^{-665}	6.0×10^{-946}
$PD^{'}$	0	9.4×10^{-43}	1.1×10^{-93}	1.6×10^{-165}	3.2×10^{-258}	3.4×10^{-371}	8.0×10^{-506}	2.4×10^{-662}	1.0×10^{-942}

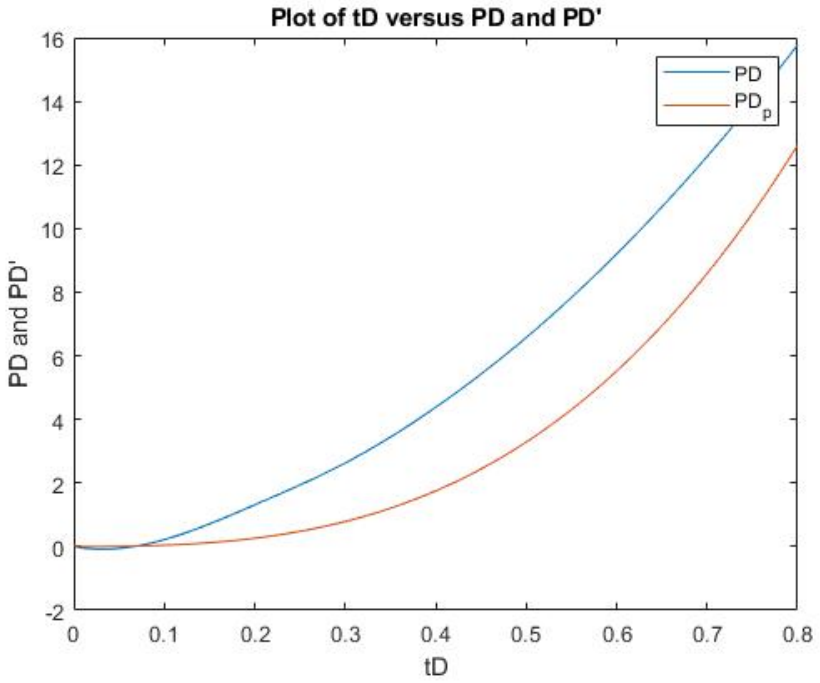

Figure 10: Variation of Dimensionless time with Dimensionless Pressure and Dimensionless Pressure derivative at pseudoradial flow

In figure 13, as dimensionless time increases, dimensionless pressure is a constant, dimensionless pressure derivative is a straight line, dimensionless reservoir width decreases and dimensionless height decreases. This results shows that dimensionless time is inversely proportional to both dimensionless reservoir width and dimensionless height. Since the pressure is a constant shows that the production of petroleum oil and gas is low, therefore the producing well is shut down for a build up. Late linear flow has a gradient of 1.

Conclusion

The creation of a four well test analysis model that analyzes reservoir characteristics and horizontal well performance using an instantaneous source and Green's function with Newmann's product. Early radial, early linear,

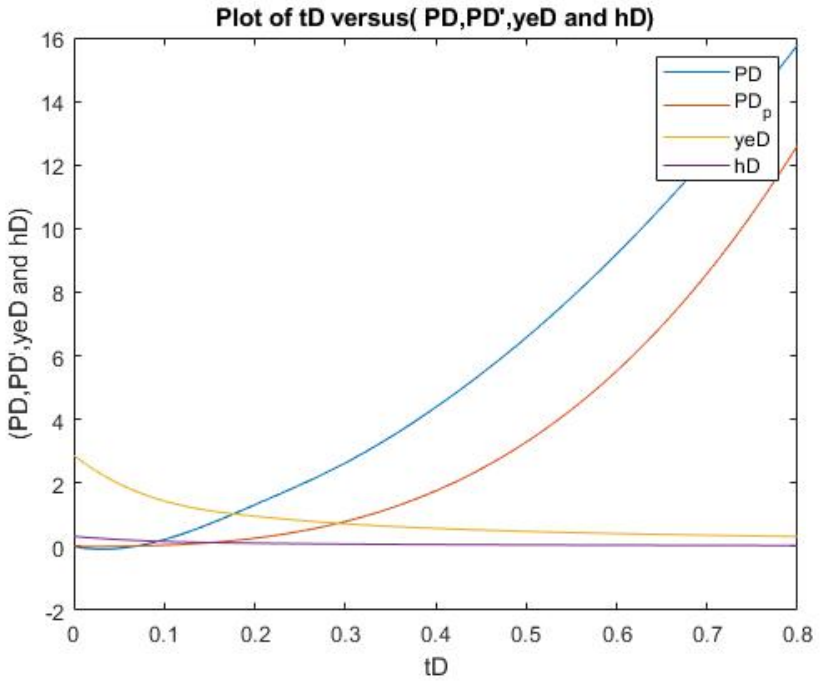

Figure 11: Variation of Dimensionless time with Dimensionless Pressure, Dimensionless Pressure derivative, Dimensionless reservoir length and pay thickness at pseudoradial flow

pseudoradial, and late linear flow are the models for the four flow periods respectively.

The four flow period has been solved by integration. The results obtain shows that as dimensionless time increases, dimensionless pressure increases, and dimensionless pressure derivative is a constant. This results shows that dimensionless time is directly proportional to dimensionless pressure. Dimensionless pressure exhibits an upward trend while the flattening of the curve for the dimensionless pressure derivative indicates the prevalence of the early radial period as expected from conventional methods. During this flow period is the period when the well is initially open for production. The production of petroleum, oil and gas is highest at this period. Early radial flow has a zero gradient. During early linear flow, as dimensionless

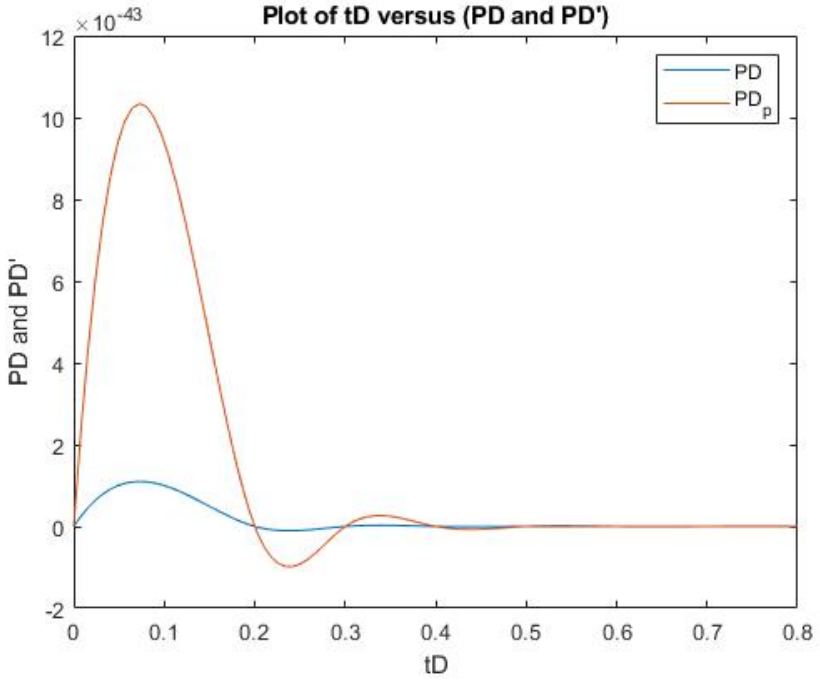

Figure 12: Variation of Dimensionless time with Dimensionless pressure and dimensionless pressure derivative at late linear flow

time increases, dimensionless pressure increases and dimensionless pressure derivative is a straight line, which implies that early linear flow has a gradient of 1. This results shows that dimensionless time is directly proportional to dimensionless pressure. The production of petroleum, oil and gas is higher. The time that early linear flow starts occurring might not be delay. During pseudoradial flow as dimensionless time increases, dimensionless pressure increases, dimensionless pressure derivative is not a perfect straight line, dimensionless reservoir width decreases and dimensionless height is a constant. This results shows that dimensionless time is directly proportional to dimensionless pressure and inversely proportional to dimensionless reservoir width. Dimensionless pressure and dimensionless pressure derivative exhibits an upward trend, while the line which is not a perfect straight line of the curve

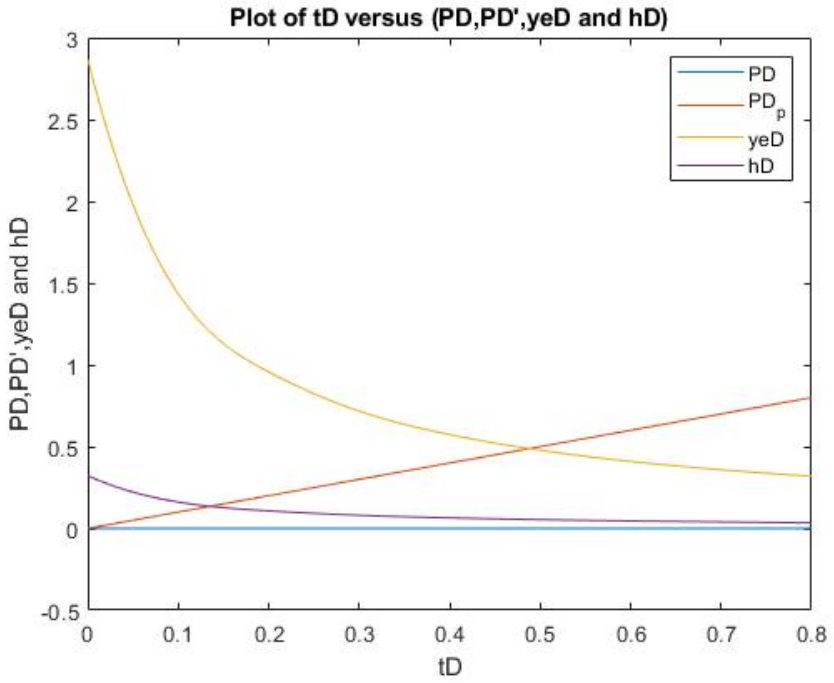

Figure 13: Variation of Dimensionless time with Dimensionless Pressure, Dimensionless Pressure derivative, Dimensionless reservoir width and dimensionless pay thickness at late linear flow

for dimensionless pressure derivative indicates the prevalence of the pseudoradial flow period as from conventional methods, because pseudoradial flow has a bigger effect of the well which indicates that the starts of pseudoradial will be delay as the reservoir width decreases. During late linear flow as dimensionless time increases, dimensionless pressure is a constant, dimensionless pressure derivative is a straight line, dimensionless reservoir width decreases and dimensionless height decreases. This results shows that dimensionless time is inversely proportional to both dimensionless reservoir width and dimensionless height. Since the pressure is a constant shows that the production of petroleum oil and gas is low, therefore the producing well is shut down for a build up. Late linear flow has a gradient of 1.

Dimensionless Parameters

This research has used dimensionless parameters to obtain the values of parameters in table 1. From table 1 the length of the well was assumed to be stretched from 250m to 2250. The values of the parameters L_D, h_D, z_D, z_{wD}, x_{eD}, z_{eD}, and r_{wD} were obtained below.

The parameters listed below helps to simplify calculations.

$i_D = \frac{2i}{L}\sqrt{\frac{k}{k_i}}$

$i_{wD} = \frac{2i_w}{L}\sqrt{\frac{k}{k_i}}$

$i_{eD} = \frac{2i_e}{L}\sqrt{\frac{k}{k_i}}$

$h_D = \frac{2h}{L}\sqrt{\frac{k}{k_z}}$

$L_D = \frac{L}{2h}\sqrt{\frac{k}{k_x}}$

$h_D = \frac{1}{L_D}\sqrt{\frac{k^2}{k_x k_z}}$

$r_{wD} = z_D - z_{wD}$

The variable $i = x, y, z$

Abbreviations

SYMBOL	MEANING
ADB	African Development Bank

BHP	Bottom hole pressure
IEA	International Energy Agency
OECD	Organization for Economic Co-operation and Development

List of Symbols

P_D	Dimensionless pressure
P'_D	Dimensionless pressure derivative
x_D	Dimensionless length
y_D	Dimensionless width
z_D	Dimensionless height
x	Length in the x-direction, m
x_e	Reservoir length, m
x_{eD}	Dimensionless reservoir length

x_w	Source coordinate in the x-direction, m
x_{wD}	Dimensionless source coordinate in the x-direction
y	Width in the y-direction, m
y_e	Reservoir width, m
y_w	Source coordinate in the y-direction, m
y_{wD}	Dimensionless source coordinate in the y-direction
z	Thickness in the z-direction, m
k	Reservoir permeability, m^2
k_x	Permeability along the x-direction m^2
k_y	Permeability along the y-direction m^2
k_z	Permeability along the z-direction m^2
z_w	Source coordinate in the z-direction, m
z_{wD}	Dimensionless source coordinate in the z-direction

Data Availability

The data used to support the findings of this study are available within the article and are also available from the co-authors upon request.

Conflicts of Interest

The authors declare that they have no conflicts of interest.

References

Adewole, E. (2009). The use of source and green's functions to model pressure distribution in a bounded layered reservoir with lateral wells, part ii: General solutions. *Journal of the Nigerian Association of Mathematical Physics*, *15*.

Akin, S. (2015). Design and analysis of multi-well interference tests. In *Proceedings of the world geothermal congress, melbourne, australia* (pp. 19–25).

Bakary L. Marong, P. R. K., & Otieno, A. K. (2022). Well test analysis of a horizontal well in a completely bounded isotropic reservoir. *International Journal of Mathematics Trends and Technology*, *68*(8), 46–66.

Cheng, Y. (2003). *Pressure transient testing and productivity analysis for horizontal wells.* Texas A&M University.

Duan, Y.-G., Ren, K.-Y., Fang, Q.-T., Wei, M.-Q., Dejam, M., & Chen, W.-H. (2020). Pressure transient analysis for a horizontal well in heterogeneous carbonate reservoirs using a linear composite model. *Mathematical Problems in Engineering*, *2020*.

Eiroboyi, I., & Obeta, P. (2014). The performance of a vertical well subject to edge water drive. In *Advanced materials research* (Vol. 1025, pp. 974–978).

Eiroboyi, I., & Wilkie, S. (2017). Comparative evaluation of pressure distribution between horizontal and vertical wells in a reservoir (edge water drive). *Nigerian Journal of Technology*, *36*(2), 457–460.

Escobar, F. H. (2018). Well test analysis for hydraulically-fractured wells. *Exploitation of Unconventional Oil and Gas Resources-Hydraulic Fracturing and Other Recovery and Assessment Techniques*, 80996.

Gao, Y., Rahman, M. M., & Lu, J. (2021). Novel mathematical model for transient pressure analysis of multifractured horizontal wells in naturally fractured oil reservoirs. *ACS omega*, *6*(23), 15205–15221.

Idudje, E., & Adewole, E. (2020). A new test analysis procedure for pressure drawdown test of a horizontal well in an infinite-acting reservoir. *Nigerian Journal of Technology*, *39*(3), 816–820.

Igba, S., Akanji, L., & Onwuliri, T. (2019). Horizontal versus vertical wells interference in hydraulically fractured shale reservoirs. *Journal of Oil, Gas and Petrochemical Sciences*.

Li, X.-P., Yan, N.-P., & Tan, X.-H. (2014). Characteristic value method of well test analysis for horizontal gas well. *Mathematical Problems in Engineering*, *2014*.

Liu, J., Liu, P., Li, S., & Wang, X. (2019). A mathematical model and semi-analytical solution for transient pressure of vertical fracture with varying conductivity in three crossflow rectangular layers. *Energy Exploration & Exploitation*, *37*(1), 230–250.

Mohammed, I., Olayiwola, T. O., Alkathim, M., Awotunde, A. A., & Alafnan, S. F. (2021). A review of pressure transient analysis in reservoirs with natural fractures, vugs and/or caves. *Petroleum Science*, *18*(1), 154–172.

Nie, R.-S., Guo, J.-C., Jia, Y.-L., Zhu, S.-Q., Rao, Z., & Zhang, C.-G. (2011). New modelling of transient well test and rate decline analysis for a horizontal well in a multiple-zone reservoir. *Journal of Geophysics and Engineering*, *8*(3), 464.

Nzomo, T., Adewole, S., Awuor, K., & Oyoo, D. (2021). Mathematical description of a bounded oil reservoir with a horizontal well. *African Journal of Pure and Applied Sciences*, *2*(1), 67–76.

Nzomo, T. K., Adewole, S. E., Awuor, K. O., & Oyoo, D. O. (2022). Performance of a horizontal well in a bounded anisotropic reservoir: Part i: Mathematical analysis. *Open Engineering*, *12*(1), 17–28.

Ogbamikhumi, A., & Adewole, E. (2020). Pressure behaviour of a horizontal well sandwiched between two parallel sealing faults. *Nigerian Journal of Technology*, *39*(1), 148–153.

Oloro, J. O., & Okpeki, U. K. (2021). Model to study pressure behavior of horizontal well subjected by both bottom water and gas cap at late time. *Advances in Dynamical Systems and Applications*, *16*(1), 59–66.

Ölz, S., Sims, R., & Kirchner, N. (2007). *Contribution of renewables to energy security*. OECD/IEA Paris.

Orene, J., & Adewole, E. (2020). Pressure distribution of a horizontal well in a bounded reservoir with constant pressure top and bottom. *Nigerian journal of Technology*, *39*(1), 154–160.

Ouyang, W., Sun, H., & Han, H. (2020). A new well test interpretation model for complex fracture networks in horizontal wells with multistage volume fracturing in tight gas reservoirs. *Natural Gas Industry B*, *7*(5), 514–522.

Pershin, V., Molero, J. C., & de Gracia, F. P. (2016). Exploring the oil prices and exchange rates nexus in some african economies. *Journal of Policy Modeling*, *38*(1), 166–180.

Sabila, T., & Habte, A. (2017). Pressure transient behaviour of horizontal wells in a bounded reservoir with gas cap and aquifer. In *Icipeg 2016: Proceedings of the international conference on integrated petroleum engineering and geosciences* (pp. 709–719).

Soleimani, R., Jahanpeyma, Y., & Salehian, M. (2019). Analysis of horizontal well productivity in tight gas formations and its sensitivity to

reservoir properties. *Journal of Petroleum Exploration and Production Technology*, *9*(2), 1237–1244.

Wang, M., Fan, Z., Zhao, W., Ming, R., Zhao, L., Tan, C., ... Li, W. (2021). Inflow performance analysis of a horizontal well coupling stress sensitivity and reservoir pressure change in a fractured-porous reservoir. *Lithosphere*, *2021*(Special 1), 7024023.

Zhang, J., Cheng, S., Di, S., Gao, Z., Yang, R., & Cao, P. (2021). A two-phase numerical model of well test analysis to characterize formation damage in near-well regions of injection wells. *Geofluids*, *2021*.

Zhao, Z., Li, Y., Jiang, T., Hu, D., Zhang, L., & Ma, R. (2022). Analysis and application of horizontal well test in low permeability porous carbonate reservoir. *Processes*, *10*(8), 1545.

Zhuo, L., Yu, J., Zhang, H., & Zhou, C. (2021). Influence of horizontal well section length on the depressurization development effect of natural gas hydrate reservoirs. *Natural Gas Industry B*, *8*(5), 505–513.